PCCP

Accepted Manuscript

ROYAL SOCIETY OF CHEMISTRY

www.rsc.org/pccp

Journal Name

ARTICLE TYPE

Cite this: DOI: 10.1039/xxxxxxxxxx

Signatures of bond formation and bond scission dynamics in dissociative electron attachment to methane

N. Douguet,*[a] D. S. Slaughter,[b], H. Adaniya,[b†], A. Belkacem,[b] A. E. Orel,[a] and T. N. Rescigno[b]

Received Date
Accepted Date

DOI: 10.1039/xxxxxxxxxx

www.rsc.org/journalname

We present a combined experimental and theoretical investigation of the dynamics and angular dependence of dissociative electron attachment to methane. We show that a triply degenerate (T_2) Feshbach resonance is responsible for the broad 10 eV dissociation peak in methane. This resonance alone is shown to correlate asymptotically to the various dissociation channels observed experimentally. The molecular-frame entrance amplitude for electron attachment is calculated for each component of the threefold degenerate resonance. By investigating the topology of the anion potential energy surfaces, we deduce the main pathways to two- and three-body breakup channels involving both bond scission and bond formation. The computed fragment angular distributions reproduce the main trends of the experimental measurements.

1 Introduction

The role of transient anion states, in particular resonances with dissociative character, has been shown to play a crucial role in the radiation-induced chemistry of biomolecules. In addition, dissociative electronic attachment (DEA) is a reaction essential to understanding the chemistry of various diffuse media, such as interstellar clouds, planetary atmospheres, and plasmas. Ion momentum imaging techniques, such as COLTRIMS (COLd Target Recoil Ion Momentum Spectroscopy) [1], provide access to vital information on the DEA of neutral molecules. Indeed, the measured angular distribution of ejected ionic fragment momenta relative to the incident electron direction represents a unique fingerprint of a particular dissociation event [2–5]. In the favorable case of prompt dissociation, characterized by the existence of predominant dissociation pathways, electron-molecule scattering calculations can tie the observed angular distributions to specific dissociation mechanisms, as shown recently in DEA to methanol [6] and acetylene [7].

Methane is a candidate of considerable interest for a detailed investigation of DEA, not only for its importance in planetary atmospheres and technological plasmas, but also because its dissociation mechanisms remain something of a mystery. The recent experimental study of Ram and Krishnakumar [8] revealed a high-level of complexity in the DEA mechanism of methane. They measured a broad dissociation peak, extending from 8 to 12 eV and centered at about 10 eV electron energy, from which both H^- and CH_2^- fragments can be formed. In addition, their measurements depict two very distinct H^- kinetic energy release (KER) peaks, suggesting the possibility of two- and three-body channel breakups in the same electron energy range. Consequently, a full description of DEA to methane requires a theoretical investigation that can predict the observed angular distributions for distinct fragment products, and the distributions corresponding to different KER. These ingredients, combined with the growing interest towards the role of conical intersections in chemistry, make DEA to methane a particularly rich and challenging process to investigate.

There are numerous past theoretical and experimental studies on low-energy electron-methane collisions and they have recently been reviewed by Song *et al.* [9]. Of those studies many have focused on elastic and inelastic scattering, with particular emphasis on very low energies where there is a Ramsauer-Townsend minimum and vibrational excitation [10–33]. Previous studies of DEA have been limited to the work of Krishnakumar *et al.* [8,34,35], Hoshino *et al.* [36,37] and an earlier study on total ion yields by Sharp and Dowell [38]. On the theoretical side, the broad maximum in the elastic cross section near 8 eV has been attributed to a shape resonance with predominantly d-wave character. However, little seems to be known about the attachment process and the subsequent dissociation dynamics. The photodissociation of methane, which presents intrinsic similarities with the DEA mechanism, already represents a particularly difficult problem to tackle, mainly due to the complexity of the multi-dimensional potential energy surfaces of excited methane, the

[a] Department of Chemical Engineering and Materials Science, University of California, Davis, CA 95616, USA.
[b] Chemical Sciences Division, Lawrence Berkeley National Laboratory, Berkeley, CA 94720, USA.
† Present address: Quantum Wave Microscopy Unit, Okinawa Institute of Science and Technology, Okinawa, Japan.

presence of triply-degenerate electronic states, and conical intersections[39].

In this communication, we present new *ab initio* theoretical results for the dynamics of three different breakup channels resulting from DEA to methane at the broad resonance that peaks at 9.9 eV collision energy. These results are compared to our anion fragment momentum imaging experimental results for all three breakup channels and with the experimental data of Ref.[8] for the two channels producing H^-.

2 Experimental setup

The anion fragment momentum imaging experiments were performed using a DEA reaction microscope, which was previously described in detail[40]. Briefly, a low-energy pulsed electron beam, with an energy spread measured to be about 0.8 eV full width at half maximum (FWHM), was produced by a tunable electron gun and guided by a coaxial magnetic field to intersect orthogonally with a methane (CH_4) or deuterated methane (CD_4) effusive molecular beam. The electron energy resolution is usually broad for imaging experiments to keep a high rate of DEA collisions. We note that the lowest vibrational mode of methane is 1367 cm^{-1} (0.17 eV) which implies that at room temperature the population of vibrationally excited species is negligible. Typically 100 ns after each electron pulse was allowed to transit the spectrometer, all anions formed in the interaction volume, defined as the intersection of the effusive beam and the electron beam, were extracted by a field of 24 V/cm into the position- and time-focusing spectrometer. Scattered electrons were prevented from entering the spectrometer through deflection by the magnetic field and by the extensive spectrometer and detector shielding, which also capacitively decoupled the detector from the pulsed field. Fragment ion momentum coordinates were encoded in the position and arrival times of the anions, as detected by a position- and time-sensitive detector consisting of a microchannel plate and delay-line anode, and recorded event-by-event. This position and time sensitivity enabled both three-dimensional momentum imaging and separation of the singly charged fragment anions. The performance and calibration of the spectrometer were periodically checked against the well-characterized momentum spectrum of O^- from DEA to O_2[40].

3 Theoretical approach

Our theoretical treatment of DEA is based on an analysis of molecular-frame scattering calculations that were performed using the complex Kohn variational method[41,42]. The ground state of methane is nominally described by a wave function with the configuration $[1a_1^2 2a_1^2 1t_2^6 3a_1^0],^1A_1$. The $^2T_2$ resonance, on the other hand, is a doubly excited Feshbach state whose parents are the $^{3,1}T_2$ excited states of methane. The negative ion resonance is formed in a collision which excites an electron from an occupied t_2 orbital and captures two electrons in the lowest unoccupied $3a_1$ molecular orbital (LUMO), to produce an anion with the nominal configuration $[1a_1^2 2a_1^2 1t_2^5 3a_1^2],^2T_2$. To achieve an accurate description of the $^2T_2$ resonance, we need a set of target molecular orbitals that can accurately describe both the ground state of methane and, more importantly, the lowest excited T_2 states which are the parents of the resonance. We started with a self-consistent field calculation on the ground-state of methane, followed by an improved virtual orbital (V_{N-1} potential) calculation to obtain a $3a_1$ molecular orbital. We used two different prescriptions to generate the occupied t_2 orbitals, both based on a calculation on the lowest triplet state of neutral methane and both giving very similar results. In one case, we carried out a multi-configuration self-consistent field calculation, averaging over the three degenerate components of the lowest T_2 triplet. Alternatively, we carried out a singles- and doubles- configurtaion-interaction calculation and obtained the averaged natural orbitals for the lowest triplet state. The $(N+1)$-electron scattering wave function was then constructed from the direct products of molecular orbitals (bound and virtual) and target states, the latter being all singlet and triplet states that could be formed using the combined set of six ($1a_1$, $2a_1$, $1t_2$ and $3a_1$) molecular orbitals. The $1a_1$ and $2a_1$ orbitals were constrained to be doubly occupied in all configurations.

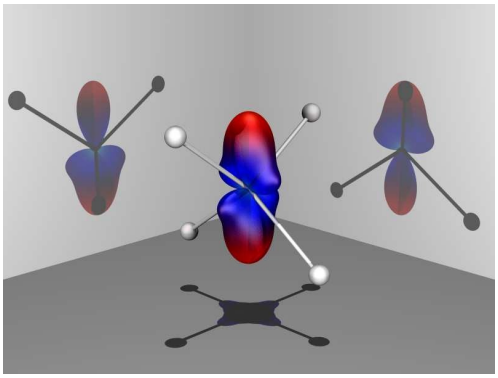

Fig. 1 3-D entrance probability $|V_z|^2$ of the T_z component.

The computed elastic cross section below 12 eV electron-energy reproduces past calculations[11,43] and experimental measurements[10], depicting a broad peak with a maximum near 8 eV electron energy. This peak, previously classified as a d-wave shape resonance[11,15], actually corresponds to a strong energy-dependent background and plays no role in DEA to methane. Electron-impact excitation of the $^{3,1}T_2$ excited states of methane, which are the parents of the Feshbach resonance, was studied by Winstead *et. al.*[44], and the vertical excitation energy to the lowest triplet-state was determined through accurate *ab initio* calculations to be about 10.6 eV.[8]

The position E_R and width Γ of the $^2T_2$ resonance was obtained by fitting the eigenphase sum from our fixed-nuclei scattering calculation at equilibrium geometry to a Breit-Wigner form, from which we obtained $E_R = 10.2$ eV and $\Gamma = 6.2$ meV. It is important to bear in mind that the measured DEA peak has an observed width of several eV. The observed width is not determined by the intrinsic fixed-nuclei electronic width of the resonance but rather by the variation of the dissociative resonance energy surface relative to the neutral target state over the Frank-Condon region. Especially in methane, our calculations show that the triply-degenerate $^2T_2$ resonance experiences strong Jahn-Teller splitting through molecular distortions, such that the resonance compo-

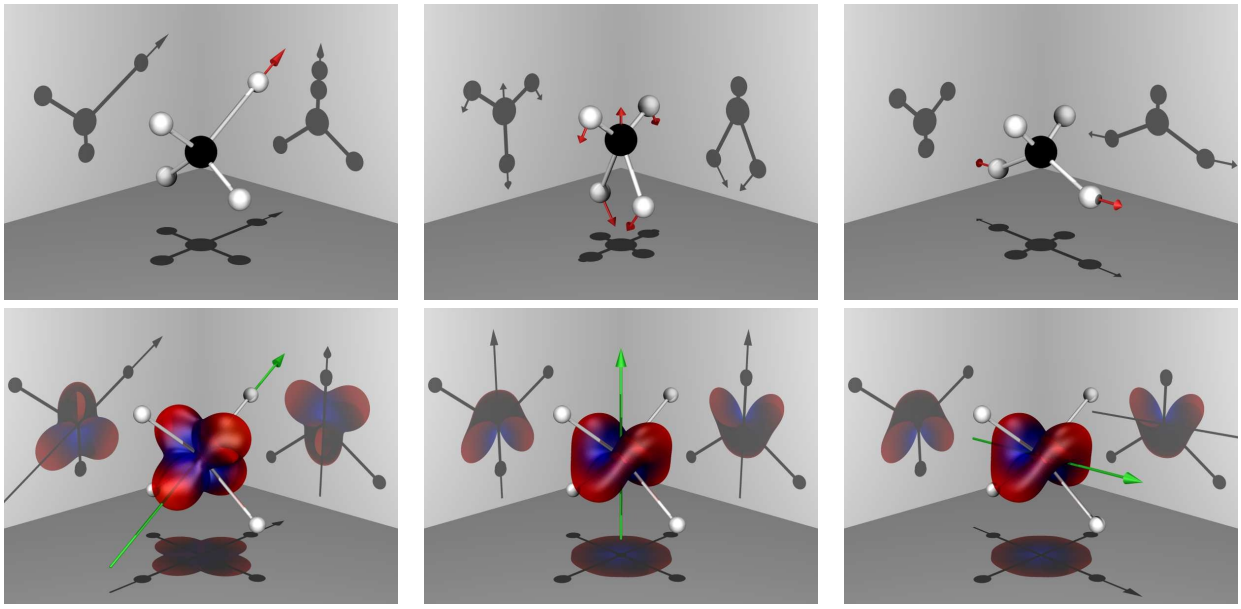

Fig. 2 Schematic representation of the main molecular distortion responsible for the experimentally observed dissociation channels (upper panels) and associated 3-D attachment probability (lower panels), with the corresponding asymptotic dissociation axis (green arrow). The channels from left to right are (i) H^-+$CH_3(\tilde{X}^2A_2'')$, (ii) CH_2^-+H_2, and (iii) H^-+H+CH_2.

nents span an energy range larger than 2 eV in the Franck-Condon region. It is unlikely that other shape- or Feshbach resonances are contributing to the broad 10 eV DEA peak. Promotion of an electron from the occupied $2a_1$ (HOMO-1) orbital would produce a state some 10 eV higher in energy that the $^2T_2$ resonance. Furthermore, we show in the following development that the $^2T_2$ resonance connects to the different fragments in their electronic ground state, such that an additional resonance in this energy domain would connect asymptotically to excited electronic states of the fragments. However, these excited states are either not accessible in the energy range considered or would lead to inconsistencies with the energetics of the observed fragments. To connect the theoretical results, computed in the body-frame, to the observed laboratory-frame angular distributions, we calculate the entrance amplitude, as described at length in ref.[45]. The entrance amplitude is a complex quantity defined as a matrix element of the electronic Hamiltonian between the resonance wavefunction Ψ_{res} and the background scattering wave function Ψ_{bg} with a plane wave incident on the target in the direction θ,ϕ:

$$\begin{aligned} V_{\bar{a}}(\theta,\phi;\mathbf{Q}) &= <\Psi_{res}(\mathbf{Q})|H_{el}|\Psi_{bg}(\theta,\phi;\mathbf{Q})> \\ &\equiv <Q\Psi|H_{el}|P\Psi>, \end{aligned} \tag{1}$$

where $\mathbf{Q}$ labels the internal coordinates of the molecule and the integration implied is over the electronic coordinates.

Rather than attempt a direct calculation of the PQ matrix element, which is complicated by the fact that the background wave function requires a Hamiltonian from which the resonance has been projected, we make use of the form of the $S-$matrix near a narrow resonance, as outlined in ref.[45], and fit the computed S-matrix elements to the functional form:

$$S_{lml'm'} = S^{bg}_{lml'm'} - \frac{i\gamma_{lm}\gamma_{l'm'}}{E-E_R+i\Gamma/2}, \tag{2}$$

where $S_{lml'm'}$ has been partitioned into a slowly varying energy-dependent background part and a resonant part and the γ_{lm} are complex partial resonance widths. The accuracy of the fitting was established by checking that $\sum_{lm}|\gamma_{lm}|^2=\Gamma$, as required by the unitarity of the S-matrix[46]. The entrance amplitude can then be evaluated as:

$$V_{\bar{a}}(\theta,\phi;\mathbf{Q}) = \frac{1}{\sqrt{2\pi}}\sum_{l,m} i^l \gamma_{lm}(\mathbf{Q})Y^*_{lm}(\theta,\phi) \tag{3}$$

Assuming axial recoil holds, the angular distribution of the DEA product ions when the relative orientation of the fragments is not observed is given by

$$\frac{d\sigma_{DEA}}{d\theta} \propto \int d\phi \left|\sum_{l,m} i^l \gamma_{lm}(\mathbf{Q})Y^*_{lm}(\theta,\phi)\right|^2 \tag{4}$$

where ϕ is the angle azimuthal to the recoil axis. When the z-axis of the coordinate system in which the scattering calculations are performed is different from that in which the z-axis is the laboratory recoil axis, we perform the necessary rotation with

$$\gamma_{lm} \rightarrow \sum_{m'} D^J_{m'm}(\alpha,\beta,\gamma)\gamma_{lm'}, \tag{5}$$

where $D^J_{m'm}$ is a Wigner rotation matrix element and α,β,γ are the Euler angles which orient the molecule in the new coordinate system.

It is important to bear in mind that using the entrance amplitude to predict the angular distribution of DEA via Eq. (4) implies

that the axial recoil approximation is satisfied. The conditions for axial recoil break down with internal rotation or bending of the transient negative ion before dissociation takes place. An in-depth computational study of these dissociation dynamics would require detailed knowledge of the topologies of the relavant negative ion potential energy surfaces, which is beyond the scope of the present study. Nevertheless, as we have shown in several previous studies[5–7,47], we can use the computed entrance amplitudes to predict angular distributions, when we have theoretical evidence that points to how the recoil axis rotates following electron attachment, by simply rotating the entrance amplitude to the appropriate recoil frame before computing the angular distributions.

In order to take best advantage of the non-abelian T_d point-group symmetry, the *ab initio* calculations were performed by placing the hydrogen atoms at the corners of a cube, with the Cartesian axes passing through the center of the faces. In this manner, the three components T_x, T_y, and T_z, of the $^2T_2$ resonance transform into each other by rotation around the C_3 axes. Additionally, the obtained attachment probabilities $|V_x|^2$, $|V_y|^2$, and $|V_z|^2$ to each resonance component also transform into each other by C_3 rotation. The 3-D attachment probability of one component, $|V_z(\theta,\phi)|^2$, is presented in Fig. 1. Here, we follow the usual convention (e.g. see ref.[6]) that the polar angles (θ,ϕ) represent the orientation of the incident electron plane-wave relative to the dissociation axis in the molecular frame.

The dynamics immediately following electron attachment to the $^2T_2$ resonance is governed by the Jahn-Teller effect, i.e. the linear splitting of the energy-position of the resonance components as a function of molecular distortion. Because of their symmetry properties, methane's normal coordinates are convenient to describe the near-equilibrium nuclear displacements. Let us recall that the triply-degenerate and doubly-degenerate modes of lowest frequencies induce bending, without stretching, whereas the symmetric and highest triply-degenerate modes are responsible for stretching. Denoting Q_i ($i = x,y,$ and z) the components of one of the triply-degenerate normal modes, the elements of the resonant part of the electronic Hamiltonian H_Q between triply-degenerate electronic states transform in cyclic permutations[48,49]:

$$\langle T_i|H_Q|T_j\rangle \propto \varepsilon_{ijk}Q_k, \tag{6}$$

with ε_{ijk} the Levi-Civita symbol. In addition, note that the doubly-degenerate mode also induces linear splitting, but does not couple different components, whereas the symmetric stretching does not induce any splitting.

4 Dissociation dynamics and angular dependence

Three dissociation channels are considered in this study and their thermodynamic threshold energies are listed in Table 1.

4.1 $H^- + CH_3$

Once the electron has attached via the resonance, the most favorable pathway toward two-body dissociation corresponds to a single bond stretch, while the remaining bonds can potentially compress or bend in a symmetric fashion. Hence, the system symmetry is reduced from T_d to C_{3v}, as shown in the top left panel of Fig. 2, and the resonance splits as $T_2 = A_1 \oplus E$. The energy-position of the A_1 component goes strongly downhill, correlating asymptotically with the $H^- + CH_3(\tilde{X}^2A_2'')$ dissociation channel, whereas both E components go uphill and are not dissociative in C_{3v} symmetry. Because the A_1 component, formed as a result of excitation out of a σ(C-H) bonding sp^3 hybrid molecular orbital, is composed equally out of the T_x, T_y, and T_z components (at tetrahedral symmetry), the corresponding attachment probability is expressed as $|V_x|^2+|V_y|^2+|V_z|^2$, thus displaying tetrahedral symmetry (see bottom left panel of Fig. 2). Because this pathway is energetically favorable and corresponds to H^- anions with high kinetic energy release (KER), as observed in the present experimental data of Fig. 3 and in Ref.[8], one expects the axial-recoil approximation to be valid in this case. This expectation must be weighed against the fact that with a peak KER of roughly $\sim$ 4.2 eV, some 2 eV of energy is absorbed in internal energy of the fragments. The dissociation axis for this channel corresponds to the C_3 axis (see Fig. 2) and the computed angular distribution in Fig. 4 is obtained by averaging around this axis. However, note that one would obtain an identical angular distribution by averaging any attachment probability component, e.g. $|V_z|^2$ in Fig. 1, around the C_3 axis.

The computed angular distribution is displayed in the left panel of Fig. 4 and compared with our measurements on CH_4 and the deuterated species CD_4. For this comparison, we selected the fragment anions whose associated energies fall into the width of the high KER peak (2-6 eV, see Fig. 3) of the experiment. Also shown in Fig. 4 are the data of ref.[8] for H^- with KER larger than 4 eV. Both sets of data are taken at 10 eV electron-energy, i.e. near the peak for H^-/D^- yield. The complete description of methane DEA would necessitate time-dependent wave-packet propagation, which as we have stated is beyond the scope of this study. Alternatively, we attempted to improve the present theoretical approach with the following considerations. We first attempted to gauge the importance of target vibrational motion by computing the entrance amplitude at several geometries within the Franck-Condon region for the case of CD_4. The changes in the angular distribution were found to be negligible. On the other hand, a noticeable improvement can be made by departing slightly from the axial-recoil approximation, using a more realistic description of the dissociation dynamics. Because there exists, from the $^2T_2$ resonance, a strong Jahn-Teller effect through molecular bending, we expect a non-negligible angular spreading of the wave-packet towards geometries breaking the C_{3v} symmetry. In practice, we have obtained a sense of this spreading effect by averaging over a dissociation axis within a cone of $\Delta\theta = 30^\circ$ angle-opening around the recoil-axis. This is about a factor of two broader than the angular resolution of the experiment, which is estimated to be $< 16^\circ$

Table 1 CH_4^- dissociation channels considered in this study.

Channel	Thermodynamic threshold (eV)
$H^- + CH_3$	3.75
$CH_2^- + H_2$	3.96
$H^- + H + CH_2$	8.37

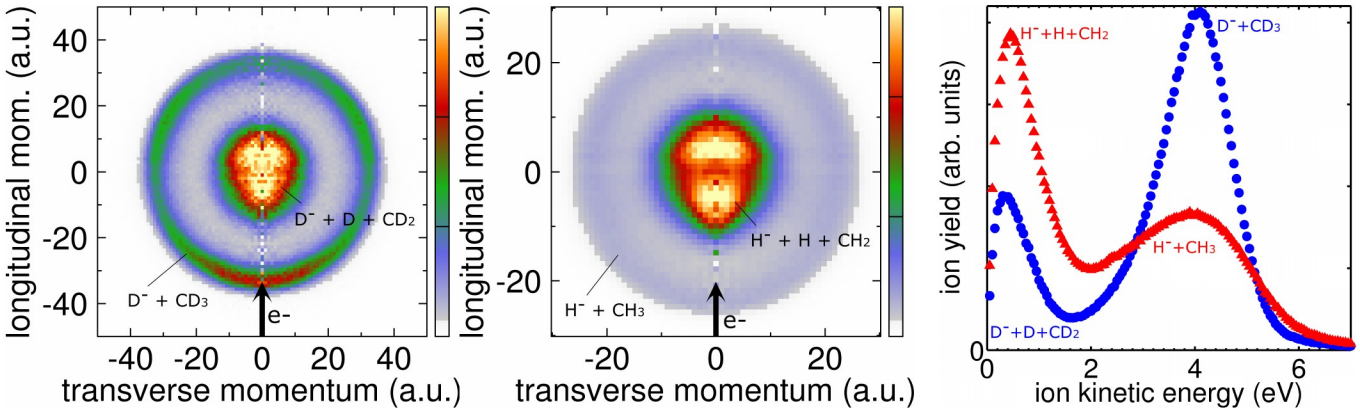

Fig. 3 Measured ion fragment momentum distribution for D^- from CD_4 (left) and H^- from CH_4 (center) for 10 eV electron attachment, with the incident electron direction denoted in each plot by an arrow. The ion yield is represented linearly by the color scale and the dissociation channel primarily contributing to each peak is as labeled. Anion fragment kinetic energy (right) for DEA to CH_4(circles) and CD_4 (triangles) for 10 eV electron attachment. The ion yields for the CD_4 and CH_4 experiments are not internormalized and have been rescaled for clarity of presentation. Statistical error bars for the ion yields are smaller than the displayed symbols.

FWHM in this case. The results are shown in Fig. 4. The theoretical angular distribution is in reasonably good agreement with our experimental measurements, depicting a broad peak at 60°, a local minimum around 120°, and strong backward scattering. From the overall shape of the 3-D attachment probability, it is clear that backward scattering dominates, which simply reflects the electron preference to attach to methane along a CH bond. While the angular distribution of ref.[8] agrees well with our calculations below 120° angles, it barely depicts any backward scattering. The reasons for the discrepancy between the two experimental results for CH_4 remain unclear. We note that while our measurements on CH_4 shows somewhat less backward scattering than in CD_4, it remains significantly larger than the data of ref.[8]. The deviations from axial recoil, correlated with a decrease in the yield of the backward-going fragment ion, are expected to be more significant with H^- than with the heavier D^-. The breakdown of the axial recoil approximation for CH_4 can be clearly seen from the lack of structure in the angular distribution.

4.2 $CH_2^- + H_2$

The detection of CH_2^- anions below the asymptotic threshold for three-body dissociation of 8.65 eV electron attachment energy[50,51] can only be associated with the fragmentation channel $CH_2^-(\tilde{X}^2B_2)+H_2$. The nuclear dynamics in this dissociation channel can be described, for the main part, in C_{2v} symmetry, choosing one of the C_2 axis as the recoil-axis. In this regard, nuclear displacements Q_i of the T_2 irreducible representation (e.g. methane normal coordinates) are the most relevant, since they create a directional asymmetry along the C_{2v} axis, which is a characteristic ultimately required in this case. On the contrary, coordinates of e irreducible representation conserve the D_{2d} symmetry of the system, with two equivalent sets of hydrogen pairs, and thus can not directly dissociate the system. Let us therefore consider one of the components, e.g. Q_z, which preserves the z axis as C_2 axis, and along which the resonance splits as $T_2 = A_1 \oplus B_1 \oplus B_2$. As can be inferred from Eq. (6), $B_1 \propto T_x - T_y$ and $B_2 \propto T_x + T_y$ will be formed near tetrahedral geometry and split linearly as a function of Q_z. On the other hand, the A_1 component, formed uniquely from the T_z component, remains flat[49]. Investigating the variations of the energy-position of the resonance components, we found that the B_2 component goes downhill as a result of either (1) a simultaneous bond stretching, or (2) an H_1-C-H_2 angle-closing of the H_1 and H_2 hydrogens. Here, note that B_2 is symmetric with respect to the H_1-C-H_2 plane. Looking at the B_2 energy-position gradient, we found that the composition of both motions is the most favorable to lower the energy, and is accompanied by a recoil of the carbon atom with a slight compression/angle-opening of the hydrogens attached to carbon, as shown in Fig. 2. Performing steepest descent calculations, we have indeed confirmed that the system goes asymptotically towards $CH_2^-(\tilde{X}^2B_2)+H_2$ and that the b_2 orbital, occupied by the lone electron and belonging to the plane of the dissociating hydrogens, transforms gradually as the b_2 orbital of $CH_2^-(\tilde{X}^2B_2)$ ground state. Therefore, this dissociation path is characterized by the scission of two C-H bonds, subsequently followed by the formation of a dihydrogen bond. From the initial large separation of the hydrogen atoms in methane (3.35 a.u.), we conclude that dihydrogen will be formed in a very excited vibrational state ($v \approx 14$). Finally, we averaged the attachment probability $|V_x|^2 + |V_y|^2$, associated with the $B_2 = T_x + T_y$ dissociative state, around the C_2 recoil-axis (see Fig. 2). The angular distribution at 8 eV is shown in the middle panel of Fig. 4 and is in striking agreement with the experimental measurements. Again, note that the exact same angular distribution would be obtained by averaging either $|V_x|^2$ or $|V_y|^2$. Above 8.65 eV electron energy, the three-body breakup channel $CH_2^-(\tilde{X}^2B_2)+H+H$ opens and the experimental results up to 10.5 eV for the CH_2^- of highest kinetic energy exhibit an increase in backward scattering, likely due to competing two-body and three-body dissociation and a breaking of the axial-recoil approximation, which could occur if the two hydrogen dissociate with significantly different momenta.

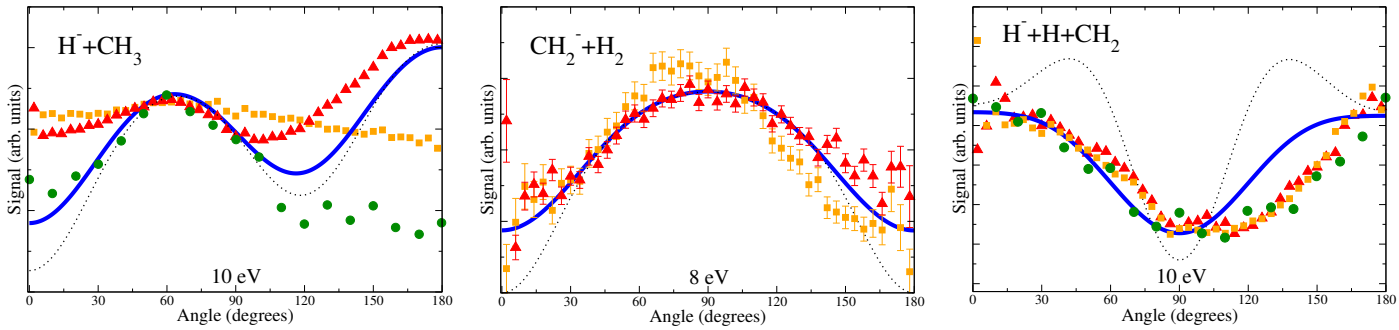

Fig. 4 Theoretical and experimental angular distributions for the main dissociation channels of methane and fully deuterated methane. Our experimental results (red triangles) for CD_4 and (orange squares) for CH_4 are presented with the data of Ref.[8] (green dots) for CH_4. The error bars for the CD_2^- data represent one standard deviation of the statistical uncertainty, while the same uncertainties for our H^- data are smaller than the displayed symbols. The theoretical angular distributions calculated at the equilibrium geometry (black dotted-line) and also averaged over a cone around the main dissociation axis (blue solid-line) as described in the text. The electron energy is shown in the bottom of each panel.

4.3 $H^- + H + CH_2$

The H^- low kinetic energy peak observed in the present experiments (see Fig. 3) and in the experiments of ref.[8] can certainly not be explained using the axial recoil approximation. In ref.[8], the authors argued that slow H^- anions could be formed as a result of sequential dissociation, first as $H^- + CH_3^*(B^2A_1')$ and then methyl would undergo rapid dissociation with ejection of a hydrogen atom. In view of our results, this possibility seems rather unlikely since the T_2 resonance does not correlate asymptotically with the $H^- + CH_3^*(B^2A_1')$ channel. Moreover, both experiments reveal the same marked trend, with forward/backward symmetry and dominant forward/backward emissions, whereas it seems unlikely that $H^- + CH_3^*(B^2A_1')$ as the first step would result in such a symmetry in the angular distribution. On the other hand, while we have demonstrated that the steepest descent correlates asymptotically with the $CH_2^-(\widetilde{X}^2B_2) + H_2$ channel, part of the wave-packet can explore other regions of the multi-dimensional surfaces. In fact, we have already indicated that simultaneous stretching of two bonds represents a motion for which the B_2 component lowers its energy. As the bond stretchs to larger values, with frozen bond angles, the b_2 orbital transforms gradually towards a $H_2^-(\sigma_u^*)$ anti-bonding molecular orbital, thus leading to H and H^- atoms dissociating in opposite directions (see Fig. 2). Let us emphasize that this path only becomes the steepest descent after a significant bond stretching. Nevertheless, pulling two hydrogens in opposite directions at methane equilibrium is already a possible path towards dissociation, though not the steepest one. Therefore, the angular distribution is again obtained by averaging $|V_x|^2 + |V_y|^2$, but now averaging around an axis in the (xy) plane. The angular distribution, shown in Fig. 4, agrees well with both experimental data, especially once averaged over a cone with $\Delta\theta = 35^\circ$ angle-opening. This is not so surprising since H^- atoms with low kinetic energy do not dissociate along a sharp direction, due to the overall spreading of the wave-packet. Finally, note that this dissociation path is the only reasonable way to explain the surprising forward/backward symmetry observed experimentally. One interesting fact is that the same B_2 component is responsible for two very different dissociative fragments, formed as a result of two very distinct pathways in the surface spanned by the B_2 component. We should finally comment on the fact, evident from the ion kinetic energy plotted in Fig. 3, that at 10 eV electron energy, the three-body $H^- + H + CH_2$ channel is relatively stronger than the two-body $H^- + CH_3$ channel, whereas for the case of D^-, the reverse is true. Let us first mention that at lower electron energies, the high KER peak for H^- actually dominates[8]. In fact, the high KER peak already exists for CH_4 at 8 eV electron energy, whereas the $H + H^- + CH_2$ channel is not yet open. As the electron energy increases, the molecular system is able to explore wider regions of the resonance energy surface and in particular the shallow path towards $H + H^- + CH_2$ dissociation. Note that CD_4 does not explore such regions as efficiently at equivalent electron energy. In addition, once the three-channel breakup $H + H^- + CH_2$ opens at 8.32 eV, dissociation towards $H^- + CH_3$ looses efficiency since the excess of energy should now be mostly transferred into H^- kinetic energy, which is an unlikely event on the view of the steepness of the dissociation path towards $H^- + CH_3$. Finally, because the H-C-H bond angle and simultaneous C-H stretch required for 3-body breakup in CH_4^- occurs faster than in CD_4^-, we could expect a higher yield from CH_4^- as the dissociating anion competes with autodetachment. The combination of the mentioned effects might explain why the dissociative flux migrate from the high to the low KER peak and why it occurs faster in the case of CH_4 than for CD_4.

5 Summary and conclusions

In summary, we have examined DEA to methane via the 10 eV resonance. We have shown that DEA in this molecule proceeds through a triply degenerate Feshbach resonance of $^2T_2$ symmetry and Jahn-Teller splitting through molecular distortions in this $^2T_2$ state induce dissociation into three different break-up channels. We have also shown that entrance amplitudes obtained from theoretical electron-methane scattering calculations, along with reasonable assumptions about the dissociation dynamics deduced from structure calculations, contain signatures of the specific bond breaking and formation dynamics of the anion. The computed angular distributions are in good agreement with our

measured differential cross sections.

6 Acknowledgements

This work is supported by the DOE Office of Basic Energy Science, Division of Chemical Sciences, Geosciences, and Biosciences under contract DE-AC02-05CH11231 and the National Science Foundation, Grant No's PHY-11-60611 and PHY-10-68785. AEO acknowledges support by the National Science Foundation, with some of this material based on work while serving at NSF.

References

1 J. Ullrich, R. Moshammer, A. Dorn, R. Dörner, L. P. H. Schmidt and H. Schmidt-Böcking, *Rep. Prog. Phys.*, 2003, **66**, 1463.
2 H. Adaniya, B. Rudek, T. Osipov, D. J. Haxton, T. Weber, T. N. Rescigno, C. W. McCurdy and A. Belkacem, *Phys. Rev. Lett.*, 2009, **103**, 233201.
3 D. J. Haxton, H. Adaniya, D. S. Slaughter, B. Rudek, T. Osipov, T. Weber, T. N. Rescigno, C. W. McCurdy and A. Belkacem, *Phys. Rev. A*, 2011, **84**, 030701.
4 D. S. Slaughter, H. Adaniya, T. N. Rescigno, D. J. Haxton, A. E. Orel, C. W. McCurdy and A. Belkacem, *Journal of Physics B: Atomic, Molecular and Optical Physics*, 2011, **44**, 205203.
5 A. Moradmand, D. S. Slaughter, D. J. Haxton, T. N. R. and C. W. McCurdy, T. Weber, S. Matsika, A. L. Landers, A. Belkacem and M. Fogle, *Phys. Rev. A*, 2013, **88**, 032703.
6 D. S. Slaughter, D. J. Haxton, H. Adaniya, T. Weber, T. N. Rescigno, C. W. McCurdy and A. Belkacem, *Phys. Rev. A*, 2013, **87**, 052711.
7 M. Fogle, D. J. Haxton, A. L. Landers, A. E. Orel and T. N. Rescigno, *Phys. Rev. A*, 2014, **90**, 042712.
8 N. B. Ram and E. Krishnakumar, *Chem. Phys. Lett.*, 2011, **511**, 22.
9 M.-Y. Song, J.-S. Yoon, H. Cho, Y. Itikawa, G. P. Karwasz, V. Kokoouline, Y. Nakamura and J. Tennyson, *J. Phys. Chem. Ref. Data*, 2015, **44**, 023101.
10 B. Lohmann and S. J. Buckmann, *J. Phys. B*, 1986, **19**, 2565.
11 B. H. Lengsfield III, T. N. Rescigno and C. W. McCurdy, *Phys. Rev. A*, 1991, **44**, 4296.
12 B. Nestmann, K. Pfingst and S. D. Peyerminhoff, *J. Phys. B*, 1994, **27**, 2297.
13 F. A. Gianturco and S. Scialla, *J. Phys. B*, 1987, **20**, 3171.
14 M. Allan, *J. Phys. B*, 2005, **38**, 1679.
15 P. Čurík, P. Čársky and M. Allan, *J. Phys. B*, 2008, **41**, 115203.
16 S. C. Althorpe, F. A. Gianturco and N. Sanna, *J. Phys. B*, 1995, **28**, 4165.
17 H. Cho, Y. S. Park, E. A. y Castro, G. L. C. de Souza, I. Iga, L. E. Machado, L. M. Brescansin and M.-T. Lee, *J. Phys. B*, 2008, **41**, 045203.
18 P. J. Curry, W. R. Newell and A. C. H. Smith, *J. Phys. B*, 1985, **18**, 2303.
19 A. L. Hughes and J. H. McMillen, *Phys. Rev.*, 1933, **44**, 876–882.
20 R. K. Jones, *J. Chem. Phys.*, 1985, **82**, 5424.
21 W. Sohn, K. Jung and H. Ehrhardt, *J. Phys. B*, 1983, **16**, 891–901.
22 J. Yuan, *J. Phys. B*, 1988, **21**, 3113–3121.
23 M. Ziółkowski, A. Vikár, M. L. Mayes, Á. Bencsura, G. Lendvay and G. C. Schatz, *J. Chem. Phys.*, 2012, **137**, 22A510.
24 N. Abusalbi, *J. Chem. Phys.*, 1983, **78**, 1213.
25 H. N. Varambhia, J. J. Munro and J. Tennyson, *Int. J. Mass Spec.*, 2008, **271**, 1–7.
26 E. Barbarito, M. Basta, M. Calicchio and G. Tessari, *J. Chem. Phys.*, 1979, **71**, 54.
27 H. Tanaka, T. Okada, L. Boesten, T. Suzuki, T. Yamamoto and M. Kubo, *Journal of Physics B: Atomic and Molecular Physics*, 1982, **15**, 3305–3319.
28 S. L. Lunt, J. Randell, J. P. Ziesel, G. Mrotzek and D. Field, *J. Phys. B*, 1994, **27**, 1407–1422.
29 D. L. McCorkle, L. G. Christophorou, D. V. Maxey and J. G. Carter, *J. Phys. B*, 1978, **11**, 3067–3079.
30 W. J Brigg, J. Tennyson and M. Plummer, *J. Phys. B*, 2014, **47**, 185203.
31 T. Nishimura and Y. Itikawa, *J. Phys. B*, 1994, **27**, 2309–2316.
32 C. T. Bundschu, J. C. Gibson, R. J. Gulley, M. J. Brunger, S. J. Buckman, N. Sanna and F. A. Gianturco, *J. Phys. B*, 1997, **30**, 2239.
33 F. A. Gianturco and D. G. Thompson, *J. Phys. B*, 1976, **9**, L383.
34 P. Rawat, V. S. Prabhudesai, M. Rahman, N. B. Ram and E. Krishnakumar, *Int. J. Mass Spec.*, 2008, **277**, 96–102.
35 P. Rawat, V. S. Prabhudesai, G. Aravind, N. Bhargavaram, M. A. Rahman and E. Krishnakumar, *J. Phys. B*, 2007, **80**, 012018.
36 C. Makochekanwa, K. Oguri, R. Suzuki, T. Ishihara, M. Hoshino, M. Kimura and H. Tanaka, *Physical Review A*, 2006, **74**, 042704.
37 M. Hoshino, Š. Matejcík, Y. Nunes, F. Ferreira da Silva, P. Limão-Vieira and H. Tanaka, *Int. J. Mass Spec.*, 2011, **306**, 51–56.
38 T. E. Sharp and J. T. Dowell, *J. Chem. Phys,*, 1967, **46**, 1530.
39 R. van Harrevelt, *J. Chem. Phys.*, 2006, **125**, 124302.
40 H. Adaniya, D. S. Slaughter, T. Osipov, T. Weber and A. Belkacem, *Rev. Scien. Instr.*, 2012, **83**, 023106.
41 T. N. Rescigno, B. H. Lengsfield and C. W. McCurdy, in *Modern Electronic Structure Theory*, ed. D. R. Yarkony, Wiley, Singapore, 1995, vol. 1, p. 501.
42 T. N. Rescigno, C. W. McCurdy, A. E. Orel and B. H. Lengsfield III, in *Computational Methods for Electron-Molecule Collisions*, ed. W. M. Huo and F. A. Gianturco, Plenum, New York, 1995.
43 F. A. Gianturco, J. A. Rodriguez-Ruiz and N. Sanna, *Phys. Rev. A*, 1995, **52**, 1257.
44 C. Winstead, Q. Sun, V. McKoy, J. L. da Silva Lino and M. A. P. Lima, *Z. Phys. D*, 1992, **24**, 141.
45 D. J. Haxton, C. W. McCurdy and T. N. Rescigno, *Phys. Rev. A*, 2006, **73**, 062724.
46 J. R. Taylor, *Scattering Theory: The Quantum Theory of Nonrelativistic Collisions*, John Wiley and Sons, Inc, 1972.

47 D. S. Slaughter, H. Adaniya, T. N. Rescigno, D. J. Haxton, A. E. Orel, C. W. McCurdy and A. Belkacem, *J. Phys. B*, 2011, **44**, 205203.

48 H. C. Longuet-Higgins, *Adv. Spectrosc.*, 1961, **II**, 429.

49 N. Douguet, V. Kokoouline and A. E. Orel, *J. Phys. B*, 2012, **45**, 051001.

50 D. G. Leopold, K. K. Murray, A. E. S. Miller and W. C. Lineberger, *J. Chem. Phys.*, 1985, **83**, 4849.

51 M. W. Chase, Jr, *J. Phys. Chem. Ref. Data, Monograph*, 1998, **9**, 1–1951.